Performance Evaluation of a Custom PID-Based Flight Controller Board for Quadcopter Stabilization

Ahmad Riyad Firdaus[1*], Daipansyah Arya Saputra[1], Ezha Tri Saputra[1], Hendawan Soebhakti[1], and Ryan Satria Wijaya[1]

[1]Robotics Engineering Technology Study Program, Electrical Engineering Department, Politeknik Negeri Batam, Batam, Indonesia

[*]Email: rifi@polibatam.ac.id

Received on 02-03-2026 | Revised on 23-06-2026 | Accepted on 26-06-2026

***Abstract*—This paper presents the design, implementation, and evaluation of a custom standalone flight controller board for quadcopter stabilization using a cascaded Proportional–Integral–Derivative (PID) control architecture. The hardware integrates an STM32F405 microcontroller, a BMI270 inertial measurement unit (IMU), and a BMP280 barometric sensor to support attitude and altitude control. Experimental evaluations included IMU accuracy testing, rig-based attitude stabilization, and real-flight trials. The IMU achieved average angular errors of ±0,24° (roll), ±0,74° (pitch), and ±0,41° (yaw), indicating reliable orientation measurement. Step-response analysis showed stable transient behavior, with overshoot values of 9,375% for roll, 25% for pitch, and 1,58% for yaw. Static attitude tests yielded mean absolute errors of 0,171° (pitch) and 0,380° (roll). Flight tests confirmed stable attitude and altitude maintenance under real operating conditions. These results demonstrate that the proposed flight controller provides reliable and scalable performance for quadcopter research and development applications.**

Keywords: Attitude Control, Cascade PID, Flight Controller, Performance Evaluation, Quadcopter,

I. INTRODUCTION

As a category of Unmanned Aerial Vehicles (UAVs), quadcopters have received considerable attention because of their high maneuverability, structural simplicity, and vertical take-off and landing (VTOL) capabilities [1]. These features make quadcopters well-suited for applications requiring precise maneuverability and autonomous operation, such as environmental monitoring, agricultural inspection, aerial mapping, and surveillance missions [2], [3].

In its conventional design, a quadcopter comprises four rotors arranged in either an "X" or "+" configuration. The motors are driven such that two rotate clockwise and the other two rotate counterclockwise, thereby generating the lift forces and control moments necessary for stable flight and maneuverability [4]. To maintain flight stability, a control system must regulate each motor's rotational speed in real time to achieve attitude and altitude stabilization. Numerous control approaches have been proposed and applied for this purpose, such as Linear Quadratic Regulator (LQR), Model Predictive Control (MPC), and Fuzzy Logic Control (FLC) [5], [6], [7]. Although numerous advanced control methods have been developed, the Proportional–Integral–Derivative (PID) controller remains the preferred control strategy due to its simplicity, practical implementation, and suitability for resource-constrained real-time embedded platforms.

The performance of a PID-based control system is influenced not only by the tuning of the controller parameters but also by the quality and capability of the flight controller hardware [8]. On many UAV platforms, commercially available flight controllers such as the Pixhawk are widely used for their high reliability and extensive software support. However, these commercial boards often have limitations in terms of input/output (I/O) flexibility, hardware customization, and adaptability to specific experimental requirements. Such limitations may restrict their applicability in research-oriented UAV development, where system customization and hardware modification are essential. Several previous studies have demonstrated that PID control can be effectively implemented on low-cost quadcopter platforms using custom-designed hardware [4], [9], [10]. Motivated by the aforementioned considerations, this research aims to develop and assess a standalone flight controller board for quadcopters, thereby improving system adaptability and supporting ongoing UAVs research and development efforts.

II. METHOD

A. Dynamic Modeling

The quadcopter UAV consists of a rigid-body structure fitted with four motor–propeller assemblies arranged symmetrically around the frame, as illustrated in Figure 1. The dynamics of the quadcopter are expressed in a body-fixed reference frame, with the *X, Y,* and *Z* axes oriented forward, laterally, and downward, respectively. Euler angles, namely roll,

parameterize the attitude of the quadcopter (ϕ), pitch (θ), and yaw (ψ) [11].

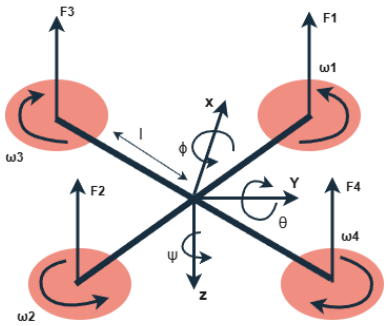

Figure 1. Quadcopter configuration

The thrust force produced by each motor is assumed to be collinear with the Z-axis of the body-fixed reference frame. The magnitude of the thrust produced by each motor depends on the square of the motor's angular velocity(ω_i^2). Consequently, the total thrust (T) quadcopter's is obtained by summing the contributions of all four motors, as expressed in Equation (1).

$$T = \mathrm{K_f}(\omega_1^2 + \omega_2^2 + \omega_3^2 + \omega_4^2) \quad (1)$$

Differences in thrust between the motors generate moments that cause the quadcopter to rotate. The pitch moment (τ_θ) is produced by the difference in thrust between the front and rear motors, while the roll moment (τ_ϕ) is produced by the thrust difference between the left and right motors. The relationships between the pitch and roll moments and the motor angular velocities are expressed in Equation (2).

$$\tau_\theta = lK_f[(\omega_1^2 + \omega_3^2) - (\omega_2^2 + \omega_4^2)]$$
$$\tau_\phi = lK_f[(\omega_1^2 + \omega_4^2) - (\omega_2^2 + \omega_3^2)] \quad (2)$$

In addition, yaw motion is generated by the reaction torque of the propellers due to the direction of motor rotation. The differences in reaction torques produce a yaw moment (τ_ψ), which is defined in Equation (3).

$$\tau_\psi = \mathrm{K_m}(\omega_1^2 + \omega_2^2 - \omega_3^2 - \omega_4^2) \quad (3)$$

This dynamic model shows that the motion of the quadcopter, including vertical movement (throttle), roll and pitch tilting, as well as yaw rotation, is entirely controlled by variations in the angular velocities of each motor. An illustration of the effect of motor speed variations on the direction of quadcopter motion is provided in Figure 2. At the same time, the definitions of the symbols used in the model equations are provided in Table I.

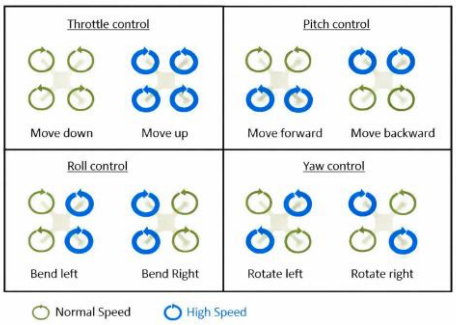

Figure 2. Quadcopter Movement

TABLE I
EXPLANATION OF SYMBOLS FOR FORMULA 1 TO 3

Variable	Description
T	Total thrust
ω_1^2	Squared angular velocity of motor 1
ω_2^2	Squared angular velocity of motor 2
ω_3^2	Squared angular velocity of motor 3
ω_3^2	Squared angular velocity of motor 4
K_f	Thrust coefficient
K_m	Moment coefficient
τ_θ	Pitch moment
τ_ϕ	Roll moment
τ_ψ	Yaw moment
l	Distance from rotor to center of mass

B. *Experimental Setup*

1) *System Design*

The system design describes the overall operational mechanism of the UAV. The schematic representation of the system implemented in this study is illustrated in Figure 3.

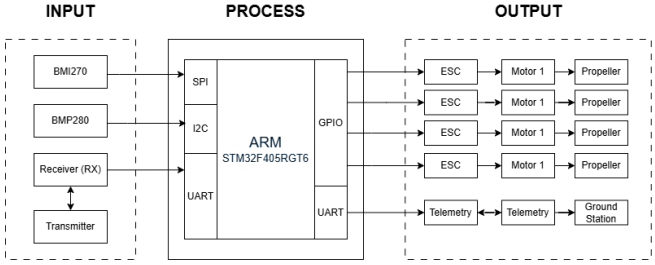

Figure 3. Diagram Blok

The remote control (RC) mode for the UAV operates via 2.4 GHz wireless communication. Control signals in the form of Pulse Width Modulation (PWM) are transmitted periodically to the radio receiver (RX) according to the positions of the control sticks and switches. The receiver then converts these signals into digital messages containing setpoint data using the S-Bus protocol [12]. The setpoint data is subsequently forwarded to the control system for processing.

The developed UAV control system is based on the STM32F405RGT6 microcontroller manufactured by STMicroelectronics. This high-performance 32-bit ARM Cortex-M4 processor operates at a maximum frequency of 168 MHz and incorporates 1 MB of flash memory along with 192 KB of SRAM, providing adequate computational resources for fast and efficient real-time data processing.

The processed setpoint data is sent to the Electronic Speed Controller (ESC), which has a current rating of 35 A, and it regulates the speed of the brushless 1000 kV motors that drive the propellers and generate lift. Additionally, the BMI270 Inertial Measurement Unit (IMU) provides information on angular orientation along three axes (X, Y, Z) and linear acceleration along three axes, serving as feedback to maintain stable motor speed [13]. Furthermore, the BMP280 pressure sensor measures atmospheric pressure, providing feedback for altitude estimation [14].

Data from the RX module and sensors are then transmitted to the Ground Control Station (GCS) via telemetry using the MAVLink communication protocol [15]. This mechanism

enables real-time monitoring of the UAV's performance, including responses to setpoints, flight stability, and environmental conditions. The real-time feedback provides operators with valuable information for assessing control system performance and optimizing system parameters to enhance flight stability and efficiency.

2) Design the Flight Controller board

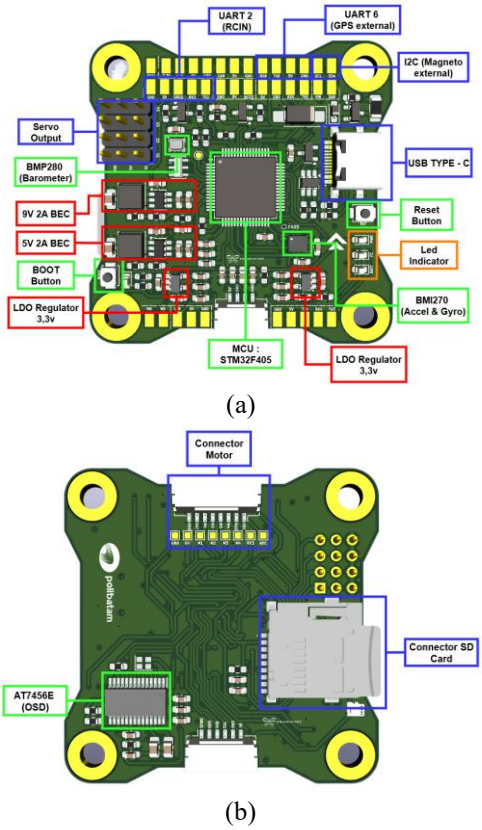

Figure 4. 3D Design PCB flight controller: (a) Top side, (b) Bottom side

Figure 4 shows the design of the Printed Circuit Board (PCB) for the flight controller (FC), developed in KiCad. The design integrates several main components, including the STM32F405 microcontroller as the central processing unit, the BMI270 inertial sensor functioning as a three-axis accelerometer and gyroscope, and the BMP280 pressure sensor used as a barometer for relative altitude measurement. In addition, the circuit is equipped with an RT9193 LDO regulator to ensure a stable power supply, along with supporting components that enhance the overall system reliability.

The FC is also equipped with various supporting features, such as the AT7456E OSD chip for flight data display, a micro-SD card slot for data logging, and multiple communication interfaces, including USB, UART, SPI, and I²C. These interfaces enable connections to external devices such as GPS modules, magnetometers, telemetry radios, and other additional sensors. Furthermore, the board provides motor/ESC outputs, PWM/servo pins, a buzzer, and LED indicators for system status indication. The PCB is designed with dimensions of 50 × 50 × 1.6 mm.

C. PID Algorithm

The basic formulation of the PID control law has been widely presented and discussed in the literature, as reported in [16], [17], [18], and is defined in Equation (4). PID control operates on the principle of minimizing the tracking error $e(t)$, defined as the deviation between the reference signal $r(t)$ and the measured system response $y(t)$ [19]. This error signal is then processed by three main control components: proportional, integral, and derivative, each weighted by the gains k_P, k_I, and k_D, respectively. The combination of these components produces the control signal $u(t)$, which is used to regulate the system and drive its output toward the desired reference value. This process illustrates how the error signal is transformed into the control action, as shown in Figure 5.

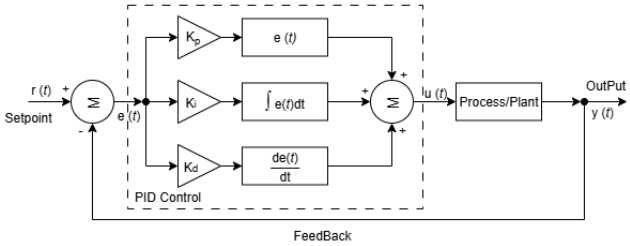

Figure 5. General block diagram of PID control system

$$e(t) = r(t) - y(t)$$

$$u(t) = K_p\, e(t) + K_i \int_0^t e(\tau)\, d\tau + K_d \frac{de(t)}{dt} \quad (4)$$

In this formulation, $e(t)$ represents the error signal, defined as the difference between the setpoint $r(t)$ and the measured output $y(t)$. The controller output is denoted by $u(t)$, while K_p, K_i, and K_d correspond to the proportional, integral, and derivative gains, respectively, and t denotes time.

To achieve optimal control performance, the gain parameters K_P, K_i, and K_d must be carefully determined through a systematic tuning process. Various tuning methods have been developed to obtain appropriate gain values. The trial-and-error tuning method [20] determines controller parameters through successive adjustments guided by system performance observations, often demanding considerable experience and multiple experimental iterations. In contrast, empirical methods such as the Tyreus–Luyben method [21] and the Ziegler–Nichols method [22] determine the PID gains based on specific system characteristics, typically derived from the critical gain and oscillation period at the stability limit. These methods provide structured guidelines for selecting control parameters and are widely adopted due to their simplicity and effectiveness in practical control applications.

The PID controller parameters were first estimated based on the Ziegler–Nichols closed-loop tuning approach. The tuning procedure was carried out by first setting K_i and K_d to zero and then progressively increasing K_p until continuous oscillatory behavior was observed. The corresponding gain at the stability limit was identified as the ultimate gain, while the oscillation period was recorded as the ultimate period. Using the obtained values, the initial PID controller parameters were calculated

following the conventional Ziegler–Nichols tuning method. Subsequently, the obtained gains were refined through a series of experimental flight tests to improve attitude stability and tracking performance. The selected controller gains were those that provided the best compromise between fast response characteristics, reduced overshoot, low steady-state error, and stable attitude control for the pitch, roll, and yaw motions. This tuning procedure ensures that the controller achieves a balance between responsiveness and robustness under actual flight conditions.

Table II presents the influence of each PID gain on system dynamics, highlighting the relationship between changes in K_p, K_i, and K_d and the resulting control performance.

TABLE II
CHARACTERISTICS OF THE PID CONTROL LAW

Parameter	Rise time	Overshot	Settling time	Steady state error
K_P	Decrease	Increase	Small change	Decrease
K_i	Decrease	Increase	Increase	Eliminate
K_d	Small change	Decrease	Decrease	Small change

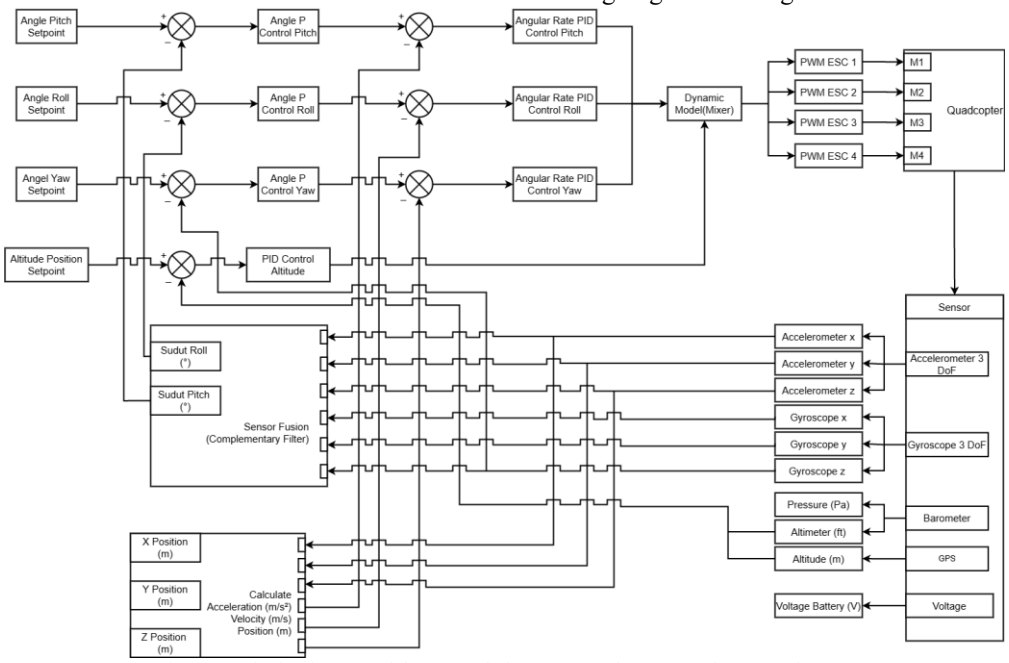

Figure 6. Block Diagram of the Cascaded PID Control Structure for a Quadcopter

Based on the results presented in Table II, increasing the proportional gain K_p generally accelerates the system response and reduces the steady-state error, but tends to increase overshoot, with a relatively small effect on the steady-state time. Meanwhile, increasing the integral gain K_i is effective in eliminating the steady-state error and can accelerate the rise time. Still, if the value is too large, it can cause greater overshoot and prolong the steady-state time due to oscillatory behavior. On the other hand, the derivative gain K_d mainly functions to improve the damping system, so it can reduce overshoot and accelerate the steady-state time, with minimal effect on the rise time and steady-state error. Therefore, in the tuning process, K_p is usually adjusted to accelerate the response, K_i is carefully increased to eliminate the steady-state error, and K_d is adjusted to suppress oscillations and improve stability around the setpoint.

D. PID Cascade Structure for UAV Quadcopter

The cascaded PID structure is proposed as the control strategy for the quadcopter UAV due to its ability to provide stable, responsive attitude control in systems with fast nonlinear rotational dynamics. Considering the high sensitivity of quadcopter motion to external disturbances and rapid variations in angular velocity, a multi-loop control strategy is required to ensure accurate stabilization. As illustrated in Figure 6, the cascaded control system employs a hierarchical closed-loop architecture consisting of an outer angle-control loop and an inner angular-rate-control loop.

The outer control loop is responsible for attitude regulation, ensuring that the quadcopter maintains the desired roll, pitch, and yaw angles during flight operations. The reference angles provided by the user or navigation system are continuously compared with the estimated actual angles obtained from inertial sensor fusion. A proportional controller processes the resulting angle error to generate a desired angular rate. action Rather than directly commanding the motors, this loop determines how fast the vehicle must rotate to achieve the desired orientation. By separating angle regulation from motor-level control, the outer loop ensures smooth and stable attitude tracking.

The inner loop performs angular rate control using feedback from accelerometer calculations. The desired angular rate generated by the outer loop is compared with the measured angular velocity, and a full PID controller processes the resulting error. The proportional term provides immediate correction, the integral term compensates for steady-state error, and the derivative term improves damping and reduces overshoot. Owing to the fast nature of rotational dynamics, the inner loop is executed at a higher frequency than the outer loop,

thereby improving disturbance attenuation and overall system stability.

In addition to attitude control, the system incorporates altitude regulation. The altitude control process begins by comparing the desired altitude with the actual altitude measured using barometric and GPS sensors. A PID controller processes the altitude error to generate a throttle command, which determines the total thrust produced by the motors. The outputs of the roll, pitch, yaw, and throttle controllers are then combined in a motor-mixing stage. The mixer distributes these control signals into individual motor commands, ensuring that the required thrust and torques are achieved simultaneously.

The cascade PID architecture offers significant advantages over a single-loop control approach. The separation of slow outer-loop dynamics and fast inner-loop dynamics enables the cascaded controller to provide superior stability, faster transient behavior, and more effective disturbance attenuation.

III. RESULT AND DISCUSSION

System testing was conducted to obtain flight controller performance data through three main stages, namely IMU sensor angle testing, attitude test rig evaluation, and flight testing.

A. Angle Testing of the IMU Sensor

The testing procedure was conducted to assess the accuracy and consistency of IMU-derived orientation angle measurements, including roll, pitch, and yaw. The system was evaluated at several predefined reference angles using calibrated angle measurement instruments. Subsequently, the sensor output was compared with the corresponding actual angles. The deviation between the reference values and the sensor measurements was defined as the measurement error, and the relative error was expressed as a percentage. Furthermore, the mean error was calculated to represent the sensor's average measurement error along each measurement axis.

1) Roll Angle Testing

TABLE III
ROLL ANGLE TEST RESULT

Measurement tools	Degree	Error	Error Percentage
60	60,24	0,24	0,4
30	30,32	0,32	1,07
15	15,08	0,08	0,53
0	0,135	0,135	N/A
-15	-14,72	0,28	1,87
-30	-30,53	0,53	1,77
-60	-59,28	0,12	0,20

Based on the roll angle test results presented in Table III, the minimum error value recorded was 0,08° while the maximum error value recorded was 0,53°. An average roll angle error of ±0,24° was obtained, indicating satisfactory measurement accuracy. In terms of percentage error, the average value was 0,97%, with the lowest and highest errors recorded at 0,20% and 1,87%, respectively.

2) Pitch Angle Testing

TABLE IV
PITCH ANGLE TEST RESULT

Measurement tools	Degree	Error	Error Percentage
60	58,7	1,3	2,17
30	28,92	1,08	3,60
15	14,1	0,9	6
0	-0,935	0,935	N/A
-15	-15,21	0,21	1,40
-30	-30,40	0,40	1,33
-60	-59,67	0,33	0,55

The results of the pitch angle test presented in Table IV show that the measurement error on the pitch axis tends to be greater than that of the roll axis. The minimum error value recorded was 0,21° while the maximum error value recorded was 1,3°. The average pitch angle error was ±0,74°, indicating a greater deviation than the roll angle measurement. Analysis of the measurement results revealed an average pitch angle error of 2,51%, with the minimum and maximum errors recorded at 0,55% and 6,00%, respectively.

3) Yaw Angle Testing

TABLE V
YAW ANGLE TEST RESULT

Measurement tools	Degree	Error	Error Percentage
0	0,8	0,8	N/A
90	89,94	0,06	0,07
180	180,22	0,22	0,12
270	269,73	0,27	0,10
360	359,32	0,68	0,19

The yaw angle test results presented in Table V show that the minimum error value recorded was 0,06°, while the maximum error value recorded was 0,8°. The average yaw angle error obtained was ±0,41°. The error percentage analysis shows that the average error in yaw angle measurement was 0,12%, with the lowest at 0,07% and the highest at 0,19%.

In general, the IMU sensor shows respectable accuracy for quadcopter stabilization. The pitch-axis error is larger than the roll and yaw errors, suggesting that sensor alignment or calibration for this axis may need further improvement. However, in real-time flight control applications, the error values stay within a reasonable range for attitude estimation.

B. Attitude Test Rig

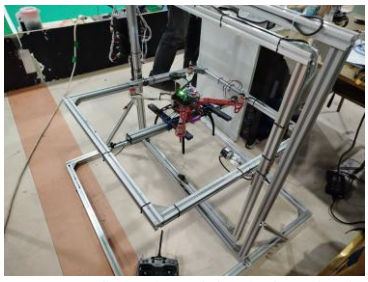

Figure 7. Configuration of the rig-based attitude control system testing setup

The objective of this test was to evaluate the effectiveness of the attitude control system and verify the implementation of the PID controller, configured with the parameters listed in Table

VI, in a controlled environment where free flight was not permitted. Through this testing, the vehicle was able to perform rotations along the roll, pitch, and yaw axes, allowing the system response to setpoint changes and external disturbances to be safely observed. Figure 7 illustrates the configuration and testing mechanism of the attitude-testing setup used during the evaluation.

TABLE VI
PARAMETER PID

Parameter	K_P	K_I	K_D
Angular Pitch	4,5	0	0
Angular Roll	4,5	0	0
Angular Yaw	3,0	0	0
Rate Pitch	0,08	0,08	0,0045
Rate Roll	0,06	0,055	0,0045
Rate Yaw	0,2	0,02	0
Altitude	0,5	0,075	0

1) *Static analysis results*

The static evaluation presented in Table VII was conducted with a 0° setpoint applied to both the pitch and roll axes to assess the attitude control system's accuracy in maintaining a horizontal position. The pitch-axis control performance showed error values ranging from 0,056° to 0,395°, with an average absolute error of 0,171°. A Root Mean Square Error (RMSE) of 0,209° was obtained, suggesting that the tracking error remained small and that the system maintained good adherence to the reference angle during testing. The RMSE is calculated using the following equation (5).

$$\text{RMSE} = \sqrt{\frac{1}{n}\sum_{i=1}^{n} e_i^2} \qquad (5)$$

In this expression, e_i corresponds to the error associated with the i-th observation, while n is the total number of collected samples. The roll-axis results showed error values between 0,008° and 1,450°, with an average absolute error of 0,380°. The higher RMSE of 0,590° relative to the pitch axis highlights larger deviations in certain measurements, particularly the 1,450° error, which contributes significantly to the quadratic mean error. Overall, based on both the mean absolute error and RMSE metrics, the attitude control system demonstrates good static performance. The pitch axis exhibits better stability and consistency, whereas the roll axis shows slightly greater variability but still maintains acceptable precision around the equilibrium condition.

These findings show that the control system can maintain a stable equilibrium condition with little steady-state error. To achieve consistent performance across all axes, the roll controller gains may need to be slightly adjusted, as indicated by the slightly higher deviation on the roll axis.

TABLE VII
ATTITUDE ANGLE TEST RESULT

Setpoint	Pitch	Pitch Error	Roll	Roll Error
0	-0,107	0,107	0,291	0,291
0	0,270	0,270	0,161	0,161
0	-0,065	0,065	0,008	0,008
0	0,118	0,118	0,111	0,111
0	-0,280	0,280	-0,031	0,031
0	-0,062	0,062	-0,797	0,797
0	-0,272	0,272	-0,283	0,283
0	-0,395	0,395	0,125	0,125
0	-0,056	0,056	1,450	1,450
0	-0,085	0,085	-0,545	0,545

2) *Pitch response analysis results*

Figure 8 illustrates that the pitch angle response following a reference change from 0° to +16° demonstrates a stable control system, whose transient performance can be assessed through quantitative analysis.

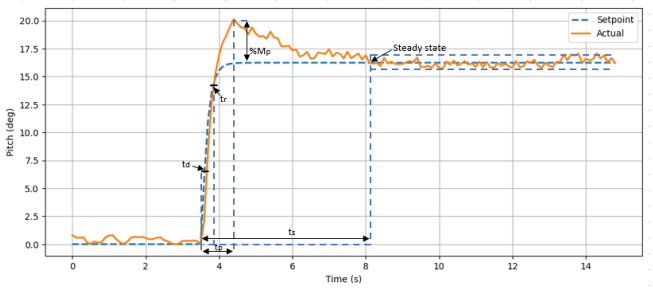

Figure 8. Pitch control system response on a quadcopter with a setpoint angle of 16 degrees

After the step input is applied, the system exhibits a delay time (t_d) of 0,2 s, representing the initial interval before the response begins to increase significantly from its initial condition. The measured rise time (t_r) of 0,4 s indicates a fast transient response, allowing the system to approach the commanded reference value efficiently. The transient response shows a maximum overshoot $(\%M_p)$ of 25% relative to the setpoint, with a maximum response value of 20°. The percentage overshoot is calculated using the following equation (6).

$$\%Overshoot = \frac{Max\ response - Setpoint}{Setpoint} \times 100\% \qquad (6)$$

In this expression, *Max Response* refers to the highest output value reached by the system after a step input is introduced, whereas *Setpoint* corresponds to the target reference value. The difference between these two values indicates how much the response exceeds the target, expressed as a percentage of the setpoint. The presence of this overshoot suggests that the system response is relatively aggressive, possibly due to a high proportional gain (K_p) or insufficient damping. The system reached its peak response at $t_p = 0{,}9$ s, which corresponds to the time required to achieve the maximum transient output before decaying toward steady-state operation. After experiencing damped oscillations, the system reaches a settling time (t_s) of 4,8 s, indicating that it ultimately stabilizes within the specified tolerance band without sustained oscillations.

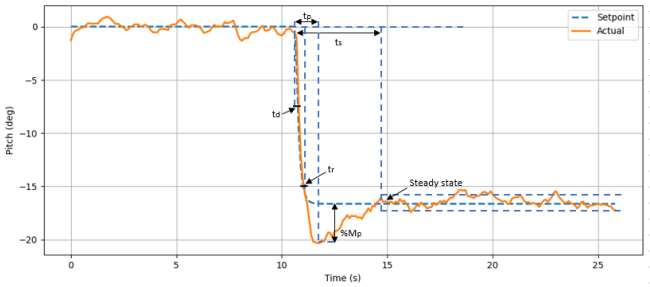

Figure 9. Pitch control system response on a quadcopter with a setpoint angle of -16 degrees

As shown in Figure 9, the system response to a negative pitch reference step from 0° to −16° presents dynamic characteristics comparable to the positive step-response case, with equivalent behavior occurring in the reverse direction. After the step input is applied, the system experiences a delay time (t_d) of 0,2 s, indicating an initial interval before the response begins to deviate significantly from its initial condition, which reflects a relatively fast initial reaction to the reference change. The rise time (t_r) is recorded at 0,4 s, demonstrating that the system can reach the negative reference value with good response speed. The transient response shows a maximum overshoot $(\%M_p)$ of 25% relative to the setpoint, with a recorded maximum response of -20°. The overshoot analysis is calculated using Equation (6). The peak time (t_p) was observed at 1 s, representing the time required for the system to reach its maximum deviation from the setpoint before the response began to decay. Subsequently, the response exhibited damped oscillations and settled within 4,1 s (t_s), indicating a faster convergence to steady-state conditions compared with the positive direction test while maintaining system stability.

The pitch controller is aggressively tuned, as evidenced by the comparatively high 25% overshoot observed in both positive and negative responses. Inadequate damping from the derivative component and a dominant proportional gain are probably the causes of this behavior. The oscillatory behavior before settling indicates that the transient response compromises stability, even though the system achieves a short rise time. The damping performance of the pitch axis is inferior to that of the roll and yaw axes, indicating that additional controller optimization, especially of the derivative term and cascaded control parameters, may be necessary.

3) Roll response analysis result

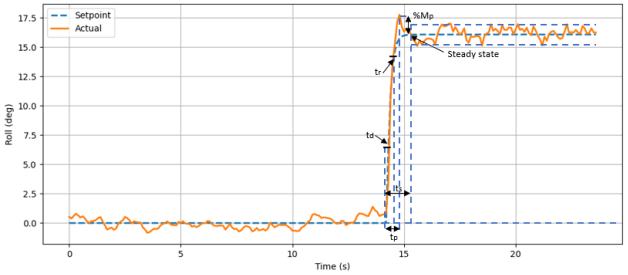

Figure 10. Roll control system response on a quadcopter with a setpoint angle of 16 degrees

As shown in Figure 10, the roll angle response following a step change in the reference signal from 0° to +16° exhibits stable dynamic behavior with a rapid transient response and effective damping characteristics. After the step input is applied, the system exhibits a delay time (t_d) of 0,2 s, indicating the initial interval before the response begins to increase significantly from its initial condition. The rise time (t_r) is recorded at 0,5 s, indicating that the system can reach the reference value at an adequate rate. The system achieved its peak response at $t_p = 0{,}8$ s, reaching a maximum output of 17,5° before transitioning toward the subsequent response phase. The magnitude of the overshoot is obtained by referring to Equation (6), resulting in a maximum overshoot $(\%M_p)$ of 9,375% relative to the setpoint. This relatively small overshoot indicates that the system exhibits better damping characteristics than the previous pitch response, as the deviation from the reference value is not significant. After reaching the peak, the system response decreases and enters a damping phase until it approaches steady-state conditions, with a settling time (t_s) of 1,9 s, indicating that the system quickly returns and stabilizes around the reference value.

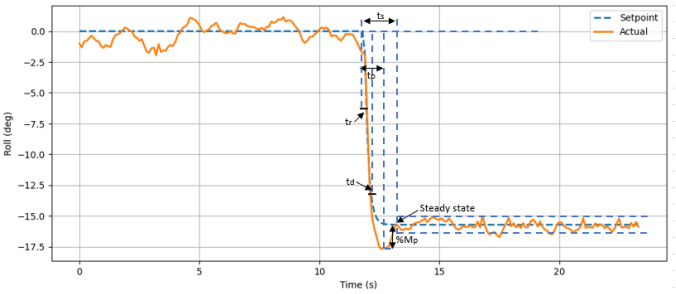

Figure 11. Roll control system response on a quadcopter with a setpoint angle of -16 degrees

As shown in Figure 11, the roll angle response to a negative step command from 0° to −16° was analyzed to verify the symmetry of the control dynamics and the consistency of system performance relative to the positive step-response case. Overall, the response exhibits stable dynamics with fast, well-damped transients, indicating that the direction of the reference change does not significantly influence the system's behavior. After the step input is applied, the system exhibits a delay time (t_d) of 0,2 s, representing the initial interval before the response begins to change noticeably. The rise time (t_r) is recorded at 0,6 s, slightly higher than the positive-direction case but still within an acceptable performance range. The peak time (t_p) occurs at 1 s with a maximum response of −17,5°, resulting in a percentage overshoot calculated using Equation (6). The maximum overshoot $(\%M_p)$The obtained value was 9,375%. This value indicates a moderate transient deviation beyond the reference before stabilization, reflecting good damping characteristics without excessive oscillations. Subsequently, the system response gradually converges to steady-state conditions with a settling time (t_s) of 2,1 s.

The lower overshoot (9,375%) and quicker settling time show that the roll response has better damping properties than the pitch axis. This implies that the roll-axis PID parameters are approaching ideal tuning conditions. Furthermore, symmetrical system dynamics are indicated by the similar response behavior in both positive and negative directions, which is crucial for reliable and consistent quadcopter maneuverability.

4) Yaw response analysis results

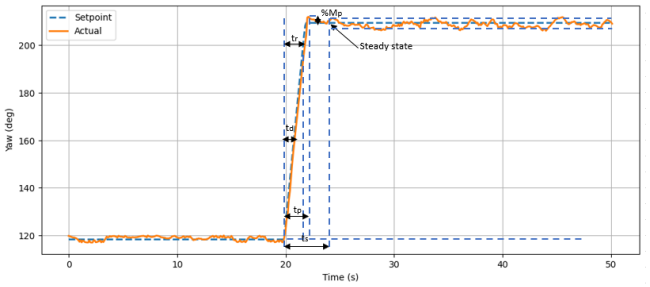

Figure 12. Yaw control system response on a quadcopter with a setpoint angle of 120° to 210°

Based on Figure 12, the yaw angle response to a gradual increase in the reference from approximately 120° to 210° shows stable, well-controlled system behavior. Compared to the pitch and roll responses, the yaw response exhibits smoother transients with minimal oscillations, indicating adequate damping and proper gain tuning in the yaw axis. After the input signal is applied, the system shows a delay time (t_d) of 0,8 s, representing the initial interval before the response begins to deviate significantly from its initial condition. The rise time (t_r) is recorded at 1,5 s, indicating that the system can track a relatively large angular change within an acceptable time. The peak time (t_p) occurs at 1,9 s, with a maximum response of 213,32°. The percentage overshoot $(\%M_p)$ is calculated using Equation (6) and is obtained as 1,58% relative to the setpoint. This very small overshoot indicates excellent damping characteristics, as the response only slightly exceeds the reference value before stabilizing. After reaching the peak value, the yaw response decreases smoothly and gradually approaches steady-state conditions. The settling time (t_s) is obtained at 3,1 s, indicating that the system reaches stable conditions.

Figure 13 shows the yaw angle response to a step increase in the reference from approximately 80° to 190°. Compared to the previous yaw test, the transient response in this case is noticeably slower, indicating that the system requires more time to adjust to a larger angular displacement from a different initial condition; however, the overall response remains stable and well-controlled without excessive oscillations. After the step input is applied, the delay time (t_d) increases to 1,6 s, followed by a rise time (t_r) of 2 s, reflecting a more gradual tracking behavior. The peak time (t_p) occurs at 2,4 s, with a recorded maximum response of 193°, after which the yaw angle slowly converges toward the desired steady-state value. The maximum overshoot $(\%M_p)$, calculated using Equation (6), remains at 1,58%, consistent with the previous yaw response, confirming that the damping characteristics of the yaw control loop are well maintained. The response finally reaches steady-state conditions with a settling time(t_s) of 4,3 s

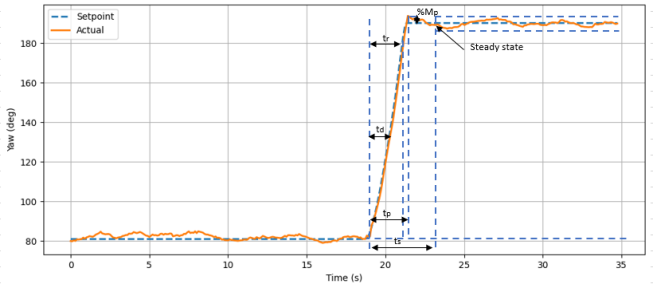

Figure 13. Yaw control system response on a quadcopter with a setpoint angle of 80° to 190°

Of all the axes, the yaw response shows the least overshoot (1,58 percent), indicating good damping performance and steady control behavior. This implies that stability is given precedence over responsiveness in the yaw controllers' conservative tuning. However, a trade-off between stability and response speed is evident in the comparatively longer rise time compared with roll and pitch, which could affect performance during quick rotational maneuvers.

C. Flight Test

(a) (b)

Figure 14. Quadcopter flight test conditions: (a) quadcopter positioned on the ground before takeoff, (b) quadcopter during flight.

As shown in Figure 14, flight experiments were conducted to assess the effectiveness of the attitude control system during real-world quadcopter operation. The objective of this experiment was to validate the performance of the PID controller configured with the parameters presented in Table VI under actual flight conditions, where the system is subjected to environmental disturbances and varying flight dynamics.

During the flight tests, attitude angle data for pitch, roll, and yaw, altitude data, and actuator output signals in the form of motor PWM were recorded and analyzed. The resulting graphs were used to evaluate the control system response to changing flight conditions across different flight phases, including takeoff, maneuvering, and landing.

Based on Figure 15, the pitch angle exhibits relatively significant fluctuations during flight, particularly between approximately 90 and 130 seconds. During this interval, the pitch angle deviation ranges from approximately ±15° to ±18°, which is associated with vertical maneuvers and thrust variations as the quadcopter adjusts its altitude. Despite these relatively large fluctuations, the pitch angle does not exhibit a divergent tendency and consistently returns toward the setpoint following disturbances. This indicates that the pitch control system can maintain the quadcopter's longitudinal stability, although the response is not yet fully smooth due to environmental disturbances and PID parameter tuning.

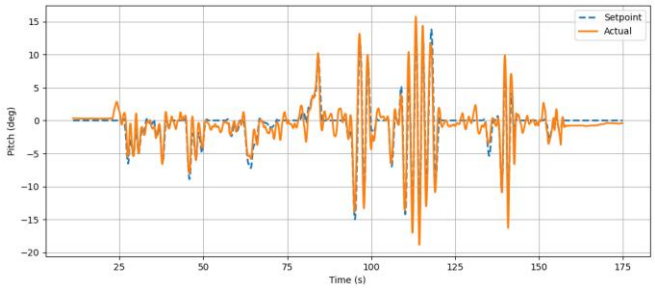

Figure 15. Pitch attitude response of the quadcopter during flight testing

Figure 16 shows oscillations with a maximum amplitude of approximately ±20° at several time intervals, particularly when the quadcopter experiences lateral disturbances or performs directional correction maneuvers. These oscillations reflect relatively large corrective responses from the control system. Nevertheless, the roll angle remains within stable limits and does not exhibit a continuous increase in amplitude. Despite the presence of disturbances, the controller successfully drives the roll angle back toward the reference value, ensuring stable lateral motion during flight.

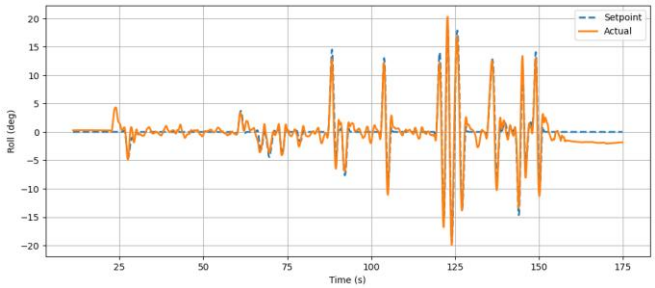

Figure 16. Roll attitude response of the quadcopter during flight testing

As illustrated in Figure 17, the response graph indicates that the actual yaw angle generally tracks the setpoint well throughout most of the testing period. However, several significant disturbances cause abrupt changes in yaw angle, particularly during the initial phase of flight and around the midpoint of the test. These large yaw variations are primarily associated with heading corrections caused by wind disturbances and directional adjustments during flight. After the occurrence of these events, the yaw response progressively returns to the reference value, demonstrating the ability of the control system to preserve heading stability under external disturbances.

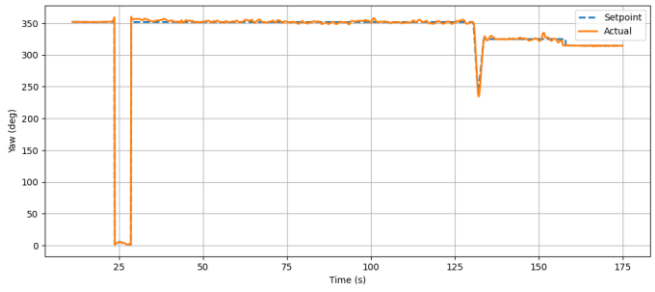

Figure 17. Yaw attitude response of the quadcopter during flight testing

Besides the analysis of attitude control performance, the effectiveness of the altitude control system was examined through the altitude and barometric altitude data shown in Figure 18. The graphs indicate that both altitude measurements exhibit similar trends, although small discrepancies are observed due to the barometric sensor's sensitivity to air pressure variations. During flight, the quadcopter can reach and maintain an altitude between approximately 1 and 4,5 meters. Motor thrust variations and air turbulence primarily cause the observed altitude fluctuations. Overall, the altitude control system maintains the quadcopter at a relatively stable altitude throughout the flight phase.

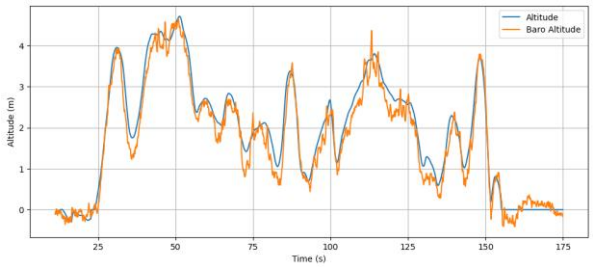

Figure 18. Altitude response based on barometric sensor measurements

The analysis of the actuator output signals is presented in Figure 19, showing that all four motors operate dynamically and respond effectively to the control system commands. The PWM values increase significantly during the takeoff phase, fluctuate throughout the flight to maintain attitude and altitude stability, and decrease again during the landing phase. Differences in PWM values among the motors reflect the real-time attitude correction process performed by the control system. No prolonged PWM saturation is observed, indicating that the actuators operate within safe operational limits throughout the testing.

The observed variations in the PWM signals are directly related to the corrective actions generated by the cascaded PID controller. During flight, attitude deviations caused by maneuvering and environmental disturbances require continuous thrust redistribution among the four motors. Consequently, each motor receives a different PWM command depending on the required roll, pitch, yaw, and throttle corrections. The dynamic but bounded PWM behavior indicates that the controller actively compensates for disturbances while maintaining sufficient control authority. Moreover, the absence of prolonged saturation demonstrates that the controller is capable of stabilizing the quadcopter without demanding excessive actuator effort. This result confirms that the proposed control system effectively translates attitude and altitude errors into appropriate motor commands, enabling stable flight operation under real-world conditions.

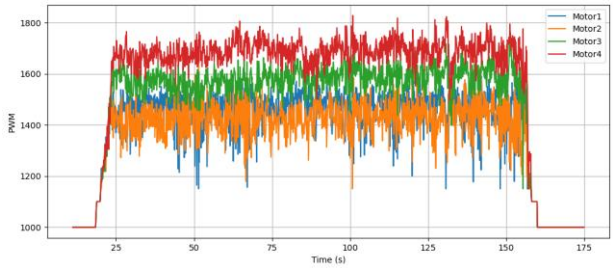

Figure 19. Motor PWM output signals.

Overall, the flight test results demonstrate that the designed PID control system can maintain the quadcopter's attitude and altitude stability under real-world flight conditions. Compared with controlled testing, the system response during flight exhibits greater fluctuations due to environmental disturbances

and flight dynamics. Nevertheless, the quadcopter remains stable and responds effectively to disturbances without losing control.

IV. CONCLUSION

This study presented the development and comprehensive performance evaluation of a custom PID-based flight controller board for quadcopter stabilization. The hardware platform was designed around the STM32F405 microcontroller and integrated with the BMI270 IMU and the BMP280 barometric sensor to ensure accurate attitude and altitude measurements. Experimental validation included sensor verification, controlled rig testing, and real-flight experiments to assess both static and dynamic performance characteristics. IMU validation results demonstrated high measurement accuracy, with average angular errors of ±0,24° for roll, ±0,74° for pitch, and ±0,41° for yaw. Static attitude testing at a 0° setpoint indicated low deviation levels, with mean absolute errors of 0,171° for pitch and 0,380° for roll. Dynamic response analysis showed fast rise times and stable transient behavior. Although the pitch axis exhibited a relatively high overshoot of 25%, the roll and yaw axes achieved better damping, with overshoot values of 9,375% and 1,58%, respectively. Real-flight experiments further verified that the cascaded PID control architecture can maintain stable attitude and altitude under practical operating conditions. Despite external disturbances such as wind and thrust variations, the quadcopter consistently returned to its reference orientation without instability or actuator saturation. Altitude was maintained within an operational range of approximately 1 m to 4,5 m, demonstrating adequate vertical stabilization. Overall, the proposed flight controller delivers stable and reliable quadcopter performance while also providing a flexible hardware platform for UAV research and future development. However, several limitations were identified in this study. The comparatively high overshoot observed in the pitch axis indicates that the PID parameters have not yet been fully optimized. In addition, the BMP280 barometric sensor is sensitive to ambient pressure fluctuations, which can reduce altitude estimation accuracy during real-flight conditions. External disturbances, particularly wind and variations in motor thrust, also significantly affect the stability and consistency of the quadcopter's response. Furthermore, the experiments were conducted under relatively moderate flight conditions, limiting the evaluation of system robustness during aggressive maneuvers or highly dynamic environments. Future research should focus on improving control performance through more advanced tuning approaches, such as adaptive PID control, fuzzy-PID methods, or optimization-based algorithms. The integration of more robust sensor fusion techniques, such as the Extended Kalman Filter (EKF), is also recommended to enhance attitude and altitude estimation accuracy. In addition, implementing complementary sensors such as GPS, optical flow, or LiDAR could further improve navigation and stabilization performance. Further flight testing involving a wider range of environmental conditions and advanced maneuvering scenarios is necessary to provide a more thorough evaluation of the proposed flight controller's robustness and operational reliability.

ACKNOWLEDGMENT

The authors gratefully acknowledge the support provided by Barelang Robotics and Artificial Intelligence (BRAIL) and the Department of Electrical Engineering, Politeknik Negeri Batam, in terms of research facilities and funding. Special thanks are also extended to the Search and Rescue Robotics Research Team at BRAIL for their technical support and constructive feedback during the research process.

REFERENCES

[1] T. C. MUSE, "VTOL AIRCRAFT," in *SAE Technical Papers*, Jan. 1961, pp. 105–112. doi: 10.4271/610178.

[2] M. Merz *et al.*, "Autonomous UAS-Based Agriculture Applications: General Overview and Relevant European Case Studies," *Drones*, vol. 6, no. 5, pp. 1–21, 2022, doi: 10.3390/drones6050128.

[3] K. V. Soumya *et al.*, "Silent Surveillance Autonomous Drone For Disaster Management And Military Security Using Artificial Intelligence," *Proc. 2023 3rd Int. Conf. Innov. Pract. Technol. Manag. ICIPTM 2023*, no. Iciptm, 2023, doi: 10.1109/ICIPTM57143.2023.10118136.

[4] A. Muhamad, S. D. Panjaitan, and R. R. Yacoub, "Design and Development of Flight Controller for Quadcopter Drone Control," *Telecommun. Comput. Electr. Eng. J.*, vol. 1, no. 3, p. 279, 2024, doi: 10.26418/telectrical.v1i3.73681.

[5] M. Okasha, J. Kralev, and M. Islam, "Design and Experimental Comparison of PID, LQR and MPC Stabilizing Controllers for Parrot Mambo Mini-Drone," *Aerospace*, vol. 9, no. 6, 2022, doi: 10.3390/aerospace9060298.

[6] B. Jiang, B. Li, W. Zhou, L. Lo, C. Chen, and C. Wen, "Quadrotor UAV," pp. 1–16, 2022.

[7] M. Azer and A. Ismail, "Attitude control of Quadrotor using enhanced intelligent Fuzzy PID controller," *Int. Res. J. Eng. Technol.*, no. May, pp. 2593–2602, 2020, [Online]. Available: www.irjet.net

[8] R. Rico, J. Rico-Azagra, and M. Gil-Martínez, "Hardware and RTOS Design of a Flight Controller for Professional Applications," *IEEE Access*, vol. 10, no. December, pp. 134870–134883, 2022, doi: 10.1109/ACCESS.2022.3232749.

[9] A. R. Al Tahtawi and M. Yusuf, "Low-cost quadrotor hardware design with pid control system as flight controller," *Telkomnika (Telecommunication Comput. Electron. Control.*, vol. 17, no. 4, pp. 1923–1930, 2019, doi: 10.12928/TELKOMNIKA.v17i4.9529.

[10] B. Sumantri, N. Tamami, Y. B. Nuraga, and B. Kurniawan, "Development of a Low-Cost Embedded Flight Controller for Quadcopter," *IES 2020 - Int. Electron. Symp. Role Auton. Intell. Syst. Hum. Life Comf.*, pp. 233–238, 2020, doi: 10.1109/IES50839.2020.9231564.

[11] E. Saif and İ. Eminoğlu, "Modelling of quad-rotor dynamics and Hardware-in-the-Loop simulation," *J. Eng.*, vol. 2022, no. 10, pp. 937–950, 2022, doi: 10.1049/tje2.12152.

[12] A. S. Hou and C. E. Lin, "Uas Delivery Multi-Rotor Autopilot Based on Ardu-Pilot Framework Using S-Bus Protocol," *Integr. Commun. Navig. Surveill. Conf. ICNS*, vol. 2022-April, pp. 1–10, 2022, doi: 10.1109/ICNS54818.2022.9771505.

[13] A. Noordin, M. A. M. Basri, and Z. Mohamed, "Sensor fusion for attitude estimation and PID control of quadrotor UAV," *Int. J. Electr. Electron. Eng. Telecommun.*, vol. 7, no. 4, pp. 183–189, 2018, doi: 10.18178/ijeetc.7.4.183-189.

[14] D. M. Ranđelović, G. S. Vorotović, A. C. Bengin, and P. N. Petrović, "Quadcopter Altitude Estimation Using Low-Cost Barometric, Infrared, Ultrasonic and LIDAR Sensors The goal," *FME Trans.*, vol. 49, no. 1, pp. 21–28, 2020, doi: 10.5937/FME2101021R.

[15] S. Atoev, K. R. Kwon, S. H. Lee, and K. S. Moon, "Data analysis of the MAVLink communication protocol," *2017 Int. Conf. Inf. Sci. Commun. Technol. ICISCT 2017*, vol. 2017-Decem, pp. 1–3, 2017, doi: 10.1109/ICISCT.2017.8188563.

[16] T. L. Mien, T. N. Tu, and V. Van An, "Cascade PID Control for Altitude and Angular Position Stabilization of 6-DOF UAV Quadcopter," *Int. J. Robot. Control Syst.*, vol. 4, no. 2, pp. 814–831, 2024, doi: 10.31763/ijrcs.v4i2.1410.

[17] S. Abdelhay and A. Zakriti, "Modeling of a Quadcopter Trajectory Tracking System Using PID Controller," *Procedia Manuf.*, vol. 32, no. 2, pp. 564–571, 2019, doi: 10.1016/j.promfg.2019.02.253.

[18] A. Sheta, M. Braik, D. R. Maddi, A. Mahdy, S. Aljahdali, and H.

Turabieh, "Optimization of pid controller to stabilize quadcopter movements using meta-heuristic search algorithms," *Appl. Sci.*, vol. 11, no. 14, 2021, doi: 10.3390/app11146492.

[19] C. Kang, B. Park, and J. Choi, "Scheduling PID attitude and position control frequencies for time-optimal quadrotor waypoint tracking under unknown external disturbances," *Sensors*, vol. 22, no. 1, 2022, doi: 10.3390/s22010150.

[20] A. Baharuddin and M. A. Mohd Basri, "Self-Tuning PID Controller for Quadcopter using Fuzzy Logic," *Int. J. Robot. Control Syst.*, vol. 3, no. 4, pp. 728–748, 2023, doi: 10.31763/ijrcs.v3i4.1127.

[21] R. Jaiswal and O. Prakash, "Classical and Modern gain estimation approach of PID controller for the pitch control of the RCTA aircraft," *INCAS Bull.*, vol. 14, no. 1, pp. 39–56, 2022, doi: 10.13111/2066-8201.2022.14.1.4.

[22] M. F. Q. Say, E. Sybingco, A. A. Bandala, R. R. P. Vicerra, and A. Y. Chua, "A Genetic Algorithm Approach to PID Tuning of a Quadcopter UAV Model," *2021 IEEE/SICE Int. Symp. Syst. Integr. SII 2021*, pp. 675–678, 2021, doi: 10.1109/IEEECONF49454.2021.9382697.